



ELSEVIER

Available online at [www.sciencedirect.com](http://www.sciencedirect.com)

SCIENCE @ DIRECT®

Journal of Computational and Applied Mathematics 192 (2006) 374–395

JOURNAL OF  
COMPUTATIONAL AND  
APPLIED MATHEMATICS

[www.elsevier.com/locate/cam](http://www.elsevier.com/locate/cam)

# A $p$ -version MITC finite element method for Reissner–Mindlin plates with curved boundaries

Christos Xenophontos<sup>a,\*</sup>, Jason Kurtz<sup>b</sup>, Scott Fulton<sup>c</sup>

<sup>a</sup>*Department of Mathematical Sciences, Loyola College, 4501 N. Charles Street, Baltimore, MD 21210-2699, USA*

<sup>b</sup>*Texas Institute for Computational and Applied Mathematics, Applied Computational and Engineering Science Building, Austin, TX 78712-1085, USA*

<sup>c</sup>*Division of Mathematics and Computer Science, Clarkson University, Potsdam NY 13699-5815, USA*

Received 23 December 2003; received in revised form 26 May 2005

## Abstract

We consider the approximation of Reissner–Mindlin plates with curved boundaries, using a  $p$ -version MITC finite element method. We describe in detail the formulation and implementation of the method, and emphasize the need for a Piola-type map in order to handle the curved geometry of the elements. The results of our numerical computations demonstrate the robustness of the method and suggest that it gives near exponential convergence when the error is measured in the energy norm. For the robust computation of quantities of engineering interest, such as the shear force, the proposed method yields very satisfactory results without the need for any additional post-processing. Comparisons are made with the standard finite element formulation, with and without post-processing.

© 2005 Elsevier B.V. All rights reserved.

*MSC:* 65N30; 65N12; 65Y99; 74S05

*Keywords:* Reissner–Mindlin plate;  $p$ -version; MITC elements; Shear locking; Curved elements

## 1. Introduction

The Reissner–Mindlin (R–M) plate model is a widely used system of partial differential equations which describes the deformation of a thin plate subject to transverse loading. This two-dimensional

\* Corresponding author. Tel.: +4106172522; fax: +4106172803.

*E-mail addresses:* [cxenophontos@loyola.edu](mailto:cxenophontos@loyola.edu) (C. Xenophontos), [kurtzj@ices.utexas.edu](mailto:kurtzj@ices.utexas.edu) (J. Kurtz), [fulton@clarkson.edu](mailto:fulton@clarkson.edu) (S. Fulton).

model often replaces the full three-dimensional elasticity problem, when the thickness of the plate is small.

The numerical approximation of the solution to the R–M plate model has received much attention in recent years. Several techniques have been proposed to alleviate the two major computational difficulties associated with this problem, namely the presence of *locking* and *boundary layer* effects. The former occurs due to the inability of the approximating spaces to satisfy certain constraints imposed on the solution as the thickness  $t$  of the plate tends to zero. The latter is due to the fact that the system of partial differential equations that describes the R–M plate model is singularly perturbed. The interplay of both phenomena is a rather complicated affair and the question of how to alleviate them *both* is still a mathematically open question (cf. [20]). Nevertheless, if one “separates” the two phenomena, then it is possible to design methods that yield very satisfactory results [25]. To deal with locking, there are two approaches one can take in the context of the finite element method (FEM): (i) enforce Kirchhoff’s constraint exactly (by using, e.g., the high-order  $p/hp$  versions of the FEM), or (ii) enforce Kirchhoff’s constraint *weakly*, by using a modified variational formulation. To deal with boundary layers, the mesh has to be properly designed and in particular it should contain *thin* (anisotropic) elements along the boundary. If the proper mesh design is combined with the  $p/hp$  version of the FEM, then exponential rates of convergence are possible.

Our goal in this article is to combine the above approaches, namely the  $p/hp$  version of the FEM with a modified formulation, and extend their applicability to R–M plates with curved boundaries. In particular, we consider the so-called *Mixed Interpolated Tensorial Components* (MITC) elements, originally introduced in [8] in terms of the  $h$  version of the FEM, and extended and analyzed in [22] in terms of the  $hp$  version. Even though in [22] the  $hp$  MITC method was defined for general curvilinear domains, the analysis was carried out only for straight-sided elements. Moreover, the only available numerical results showing the robustness of the  $hp$  MITC method are found in [2], and once more they are carried out only for straight-sided elements. (See also [3] for more on the approximation theory of  $hp$  MITC elements.) We wish to extend the results from [2] to the case of curved elements, and verify that the (original) definition of the  $hp$  MITC elements from [22] indeed works in practice when one deals with curvilinear domains. Building on the ideas used for nearly incompressible elasticity in [13], we are able to construct a  $p$  version MITC method with the following properties:

- The method performs well, independently of the thickness of plate or the error measure used, provided one uses the proper mesh design for capturing the boundary layer that is (generally) present in the solution.
- No additional post-processing is required for the accurate calculation of quantities of engineering interest.
- Curved elements are handled with the use of a Piola-type mapping.

We hope that the present article will provide the groundwork for future research on these methods, especially in establishing the observed near exponential convergence rates.

In what follows, the usual  $L^2$  inner product and norm are denoted by  $(\cdot, \cdot)_\Omega$  and  $\|\cdot\|_{0,\Omega}$ , respectively, where  $\Omega \subset \mathbb{R}^2$  with boundary  $\partial\Omega$  smooth. The usual Sobolev spaces of functions on  $\Omega$  with  $r$  generalized derivatives in  $L^2(\Omega)$  will be denoted by  $H^r(\Omega)$ , and their norms by  $\|\cdot\|_{r,\Omega}$ . Finally, the space  $H_0^1(\Omega)$  will be used to denote functions in  $H^1(\Omega)$  whose trace vanishes on  $\partial\Omega$ .

The rest of the paper is organized as follows: In Section 2 we present the R–M equations and their discretization. Section 3 details the derivation and implementation of a  $p$ -version MITC method for curved elements and Section 4 contains the results of numerical computations for two model problems. Our conclusions are presented in Section 5.

## 2. The Reissner–Mindlin plate model and its discretization

Consider the bending of a homogeneous isotropic plate of thickness  $t > 0$ , occupying the region  $\mathcal{R} = \Omega \times (-t/2, t/2)$ , where  $\Omega \subset \mathbb{R}^2$  represents the midplane of the plate, under normal load density given by  $t^3 g(x, y)$ , where  $g$  is independent of  $t$ . The equations of equilibrium for the rotation  $\vec{\phi}$  and transverse displacement  $w$  are

$$-\frac{D}{2}((1-\nu)\vec{\Delta}\vec{\phi} + (1+\nu)\vec{\nabla}\nabla \cdot \vec{\phi}) - G\kappa t^{-2}(\vec{\nabla}w - \vec{\phi}) = \vec{0}, \quad (1)$$

$$-G\kappa t^{-2}\nabla \cdot (\vec{\nabla}w - \vec{\phi}) = g, \quad (2)$$

where  $E$  is Young's modulus,  $\nu$  is Poisson's ratio,  $G = E/[2(1+\nu)]$  is the elastic shear modulus,  $D = E/[12(1-\nu^2)]$  is the modulus of flexural rigidity, and  $\kappa$  is the shear correction factor (often chosen as  $5/6$ ).

It is well known that the solution to the second-order R–M system (1)–(2) converges to the solution of the fourth-order Biharmonic equation as  $t \rightarrow 0$ , i.e., the solution to the R–M plate satisfies *Kirchhoff's constraint*

$$\vec{\nabla}w - \vec{\phi} = \vec{0}. \quad (3)$$

Practically, this means that straight fibers normal to the undeformed midplane remain straight and normal to the deformed midplane  $w(x, y)$ . This fact leads to difficulty in approximating the solution to (1)–(2) for very thin plates, because the discretization of the second-order system is being used to approximate functions that are converging to the solution of a fourth-order equation. Our goal is to obtain a discretization of (1)–(2) that performs well independently of  $t$ , on a domain with curved boundaries. In practice, one is often interested in the accurate approximation of the stress and moment resultants, such as the shear force, defined as

$$\vec{Q} = \langle Q_x, Q_y \rangle = -G\kappa t^{-2}(\vec{\nabla}w - \vec{\phi}). \quad (4)$$

We will restrict our description of the method to clamped plates, where the displacement and rotation are zero on  $\partial\Omega$ . Other boundary conditions (as in Section 4.2) may be treated similarly (see [15] for details). Our numerical results in Section 4 ahead will demonstrate the applicability of the method to other boundary conditions as well.

The standard variational formulation of (1)–(2) proceeds as usual: find  $(\vec{\phi}, w) \in [H_0^1(\Omega)]^2 \times H_0^1(\Omega)$  such that

$$\frac{D}{2}a(\vec{\phi}, \vec{\theta}) + G\kappa t^{-2}b(\vec{\phi}, w; \vec{\theta}, \zeta) = (g, \zeta)_\Omega \quad (5)$$

for all  $(\vec{\theta}, \zeta) \in [H_0^1(\Omega)]^2 \times H_0^1(\Omega)$ , where

$$a(\vec{\phi}, \vec{\theta}) = \int_{\Omega} \{(1 - \nu)(\vec{\nabla}\phi_1 \cdot \vec{\nabla}\theta_1 + \vec{\nabla}\phi_2 \cdot \vec{\nabla}\theta_2) + (1 + \nu)(\nabla \cdot \vec{\phi})(\nabla \cdot \vec{\theta})\} dA, \tag{6}$$

$$b(\vec{\phi}, w; \vec{\theta}, \zeta) = \int_{\Omega} (\vec{\nabla}w - \vec{\phi}) \cdot (\vec{\nabla}\zeta - \vec{\theta}) dA. \tag{7}$$

The standard finite element discretization of (5) consists of constructing a pair of finite-dimensional subspaces  $\vec{V}_N(\Omega) \subset [H_0^1(\Omega)]^2$ ,  $W_N(\Omega) \subset H_0^1(\Omega)$  of combined dimension  $N$  (the total number of degrees of freedom), and solving the problem: find  $(\vec{\phi}_N, w_N) \in \vec{V}_N(\Omega) \times W_N(\Omega)$  such that

$$\frac{D}{2} a(\vec{\phi}_N, \vec{\theta}) + Gkt^{-2} b(\vec{\phi}_N, w_N; \vec{\theta}, \zeta) = (g, \zeta)_{\Omega} \tag{8}$$

for all  $(\vec{\theta}, \zeta) \in \vec{V}_N(\Omega) \times W_N(\Omega)$ . The global spaces  $\vec{V}_N(\Omega)$  for the rotation and  $W_N(\Omega)$  for the midplane displacement are constructed by first partitioning the domain  $\Omega$  into a mesh  $\mathcal{M}$  of curvilinear quadrilateral and/or triangular elements  $\Omega_k$ , each of which is the image of a reference element  $\hat{\Omega}$  under an invertible element mapping  $\mathcal{F}_k : \hat{\Omega} \rightarrow \Omega_k$ . The reference element  $\hat{\Omega}$  is chosen as either the unit square  $\hat{S} = [-1, 1]^2$  or the reference triangle  $\hat{T} = \{(\zeta, \eta) \in [0, 1]^2 : \eta \leq 1 - \zeta\}$ . Then the global spaces  $\vec{V}_N(\Omega)$ ,  $W_N(\Omega)$  are defined piecewise in the following way:

(1) Polynomial spaces  $\hat{V}_{p_1}(\hat{\Omega})$  and  $\hat{W}_{p_2}(\hat{\Omega})$  are chosen on the reference elements  $\hat{\Omega} = \hat{S}$  or  $\hat{T}$ , among

$$\mathcal{Q}_{p,q}(\hat{\Omega}) = \text{span}\{\xi^i \eta^j : 0 \leq i \leq p, 0 \leq j \leq q\}, \tag{9}$$

$$\mathcal{Q}_p(\hat{\Omega}) = \mathcal{Q}_{p,p}(\hat{\Omega}), \tag{10}$$

$$\mathcal{P}_p(\hat{\Omega}) = \text{span}\{\xi^i \eta^j : 0 \leq i + j \leq p\}. \tag{11}$$

(2) The reference spaces are mapped onto each element to create the spaces

$$\vec{V}_{p_1}(\Omega_k) = \{\vec{\phi}_{p_1} = \hat{\phi} \circ \mathcal{F}_k^{-1} : \hat{\phi} \in \hat{V}_{p_1}(\hat{\Omega})\}, \tag{12}$$

$$W_{p_2}(\Omega_k) = \{w_{p_2} = \hat{w} \circ \mathcal{F}_k^{-1} : \hat{w} \in \hat{W}_{p_2}(\hat{\Omega})\}. \tag{13}$$

(3) The global spaces are then defined by

$$\vec{V}_N(\Omega) = \{\vec{\phi}_N \in H_0^1(\Omega) : \vec{\phi}_N|_{\Omega_k} \in \vec{V}_{p_1}(\Omega_k) \forall \Omega_k \in \mathcal{M}\}, \tag{14}$$

$$W_N(\Omega) = \{w_N \in H_0^1(\Omega) : w_N|_{\Omega_k} \in W_{p_2}(\Omega_k) \forall \Omega_k \in \mathcal{M}\}. \tag{15}$$

The standard discretization (8) is highly sensitive to the plate thickness  $t$ . It is well known that the standard  $h$  version exhibits complete locking, unless polynomials of degree greater than 3 are used for the approximation. Unlike the  $h$  version, the high-order  $p$  and  $hp$  versions are free of locking as  $p \rightarrow \infty$ , when the error in the energy norm is of interest (see [23] for more details). Though it has been shown that standard  $p$  and  $hp$  version methods are free of locking, rigorous analyses have only been completed for meshes consisting of rectangular and straight sided triangular elements [24]. The analysis of the  $p/hp$  version for curvilinear meshes remains open, even though numerical evidence suggests

that these methods are indeed asymptotically locking-free, even when certain curvilinear elements are used ([20,16,15]). However, standard methods do not yield satisfactory results when the moment and/or stress resultants are of interest (see, e.g., [14]). In [17] this problem was somewhat alleviated through the use of the  $p$ -version FEM along with a post-processing scheme for computing the resultants, and in particular the shear, equivalent to using the equilibrium (as opposed to the constitutive) relation. One of the main advantages of MITC methods, and the motivation behind our study, is that the need for such post-processing is eliminated since these methods approximate both the solution and the resultants well, without any additional computational effort. In addition, MITC methods have also been proven to work extremely well for the more difficult shell problem, for which curved elements are most useful (cf. [7]).

### 3. A $p$ version MITC method

So-called MITC methods reduce the adverse effect of Kirchhoff's constraint on the approximation of thin plate problems. Since their introduction in 1989 by Brezzi et al. [8], they have arguably become the "method of choice" for the approximation of plate problems. In this section we discuss the MITC formulation and its stability, as well as give details for the implementation of a  $p$ -version MITC method based on the Raviart–Thomas spaces [18].

#### 3.1. The MITC formulation and its stability

The idea behind MITC methods, and their analysis, is to rewrite problem (5) as a system of two Poisson equations and a Stokes-like system, using a Helmholtz decomposition [10]. The advantage of this approach is that (5) can be treated as three independent problems for which results are available in the literature; see [22] for more details. The first step in this process is to choose a space  $\vec{V}_N$  for the rotation, which together with an auxiliary space  $R_N$  is known to work for the (rotated) Stokes system, in the sense that

$$\sup_{\vec{0} \neq \vec{\eta} \in \vec{V}_N} \frac{(\text{rot } \vec{\eta}, q)_\Omega}{\|\vec{\eta}\|_{1,\Omega}} \geq C(h, p) \|q\|_{0,\Omega} \quad \forall q \in R_N, \quad (16)$$

with the positive constant  $C(h, p)$  depending as little as possible on the mesh width  $h$  and the polynomial degree  $p$ . In (16) the rotation operator is defined as

$$\text{rot } \vec{\eta} = \text{rot}(\eta_1, \eta_2) = \frac{\partial \eta_2}{\partial x} - \frac{\partial \eta_1}{\partial y}.$$

The next step is to project  $\vec{V}_N$ , using a reduction operator  $\Pi_N$ , onto another auxiliary space  $\vec{\Gamma}_N$  such that

$$(\text{rot}(\Pi_N \vec{\phi} - \vec{\phi}), q)_\Omega = 0 \quad \forall q \in R_N.$$

Pairs of spaces  $(\vec{\Gamma}_N, R_N)$  of this type as well known in the literature (cf. [11]), an example being the Raviart–Thomas spaces [18] we will use in our study.

The final step in defining the MITC method is to choose the space  $W_N$  such that

$$\nabla W_N = \{\vec{\phi} \in \vec{\Gamma}_N : \text{rot } \vec{\phi} = 0\},$$

and solve discrete problem: find  $(\vec{\phi}_N, w_N) \in \vec{V}_N(\Omega) \times W_N(\Omega)$  such that for all  $(\vec{\theta}, \zeta) \in \vec{V}_N(\Omega) \times W_N(\Omega)$

$$\frac{D}{2}a(\vec{\phi}_N, \vec{\theta}) + G\kappa t^{-2}b(\Pi_N \vec{\phi}_N, w_N; \Pi_N \vec{\theta}, \zeta) = (g, \zeta)_\Omega. \quad (17)$$

We now turn our attention to the pair of spaces  $(\vec{V}_N, R_N)$  for which (16) holds. When the mesh consists of quasiuniform, straight sided elements, the results of [21] provide several choices for such spaces, along with the estimate

$$C(h, p) \geq Cp^{-1/2} \quad (18)$$

for the stability constant in (16), with  $C$  independent of  $h$  and  $p$ . Using this result, the analysis of  $hp$  MITC methods for the R–M plate was presented in [22]; see also [2] for additional information and numerical experiments.

The estimate (18) on the stability constant remains valid when the elements are curved, as was shown in [12,13], provided the mesh satisfies certain (mild) conditions in addition to being quasiuniform (see [12] for specific details). Moreover, as it was shown in [13], the element mappings must be constructed with care, as will be discussed in the next subsection. Hence, in principle, if the results of [22] and [13] are combined, then a stable  $hp$  MITC method with curved elements can be obtained—in fact, this is precisely what we have achieved in practice in the present article. However, in order to prove that this method is indeed stable, one would need to extend the analysis of [22] to the case of curved elements, something that depends very strongly on the validity of the Helmholtz decomposition at the discrete level, when the mesh consists of curved elements. To our knowledge, such results are not available, and establishing them is beyond the scope of this article. Moreover, since in general the solution will contain boundary layers, the mesh must be constructed appropriately (in an anisotropic way) and include thin elements along the boundary (cf. [20]). Even though stability results for the Stokes problem with anisotropic refinement are available [19,1], they focus only on the case of straight sided elements. The stability of mixed  $hp$  methods for the Stokes problem with high aspect ratio (anisotropic) *curved* elements is still, to our knowledge, an open question. Nevertheless, once the above-mentioned tools become available then the stability of the method presented here can be established.

### 3.2. Discretization

We now focus on the discretization aspects of the method, and in particular we explain how to handle the curved element mappings. As mentioned above, we start with a known space  $\vec{V}_N$  for the rotation, and then project it, using a reduction operator  $\Pi_N$ , onto a space of polynomials (see [22] for several choices of such spaces and reduction operators). These global spaces are defined using the usual reference spaces; however, as was shown in [13], curved elements require some “special” treatment. In particular, the basis for the reference space for the rotations is “split” into two disjoint subsets corresponding to the *internal* and *external* basis functions. The external basis functions are those which are non-zero along (at least one portion of) the boundary, while the internal basis functions are zero along the boundary and non-zero in the interior (see e.g., Chapter 6 in [26]). The space spanned by the external basis functions is mapped using the usual mapping in order to ensure inter-element continuity. The space spanned by the internal basis functions is mapped using a kind of *Piola* transform (see below and [13]).

The specific choices for the spaces used here correspond to Method 4 of [22] and Method 3 of [13]. Consequently, the rotation space  $\vec{V}_N$  is defined for a mesh  $\mathcal{M}$  composed of curvilinear quadrilaterals as follows:

- (1) The reference space  $\widehat{V}_p(\widehat{S})$  on the reference square is taken to be

$$\widehat{V}_p(\widehat{S}) = [\mathcal{Q}_{p+1}(\widehat{S})]^2 = \widehat{V}_p^0(\widehat{S}) \oplus \widehat{V}_p^e(\widehat{S}).$$

The superscript 0 is used to denote the subspace of functions zero on  $\partial\widehat{S}$  (i.e., the space spanned by the internal basis functions), and  $e$  denotes functions nonzero on  $\partial\widehat{S}$  (i.e., the space spanned by the external basis functions).

- (2) The element space  $\vec{V}_p(S_k)$  is defined by

$$\begin{aligned} \vec{V}_p(S_k) &= \vec{V}_p^0(S_k) \oplus \vec{V}_p^e(S_k), \\ &= \{\vec{\phi} = J_k^{-T} \widehat{\phi} \circ \mathcal{F}_k^{-1} : \widehat{\phi} \in \widehat{V}_p^0(\widehat{S})\} \oplus \{\vec{\phi} = \widehat{\phi} \circ \mathcal{F}_k^{-1} : \widehat{\phi} \in \widehat{V}_p^e(\widehat{S})\}, \end{aligned} \quad (19)$$

where  $S_k = \mathcal{F}_k(\widehat{S})$  and  $J_k^{-T}$  is the inverse transpose of the derivative of the element mapping  $\mathcal{F}_k$ . Notice the modified mapping used for the internal shape functions.

- (3) The global space  $\vec{V}_N$  is defined by

$$\vec{V}_N = \{\vec{\phi} \in [H_0^1(\Omega)]^2 : \vec{\phi}|_{S_k} \in \vec{V}_p(S_k), \forall S_k \in \mathcal{M}\}.$$

The midplane displacement space  $W_N(\Omega)$  is obtained in the usual manner using (13) and (15) with  $\widehat{W}_p(\widehat{\Omega}) = \mathcal{Q}_p(\widehat{\Omega})$ .

The space  $\vec{V}_N$  is projected by a reduction operator  $\Pi_N$ , defined elementwise by

$$(\Pi_N \vec{\phi})|_{S_k} = \begin{cases} J^{-T}(\widehat{\Pi}_p \widehat{\phi}) \circ \mathcal{F}_k^{-1} & \text{for } \vec{\phi}|_{S_k} \in \vec{V}_p^0(S_k), \\ (\widehat{\Pi}_p \widehat{\phi}) \circ \mathcal{F}_k^{-1} & \text{for } \vec{\phi}|_{S_k} \in \vec{V}_p^e(S_k), \end{cases}$$

where the reference projection  $\widehat{\Pi}_p$  is a strategically chosen projection onto a space of polynomials. In our study, we choose the Raviart–Thomas spaces  $\mathcal{Q}_{p-1,p}(\widehat{S}) \times \mathcal{Q}_{p,p-1}(\widehat{S})$  (see [18] and [11]), even though other choices are possible, e.g. the BDFM spaces [9]. Specifically, the conditions defining  $\widehat{\Pi}_p$  are

$$\int_{\widehat{E}} ((\widehat{\Pi}_p \widehat{\phi} - \widehat{\phi}) \cdot \vec{t}) \widehat{v} = 0, \quad \text{for all } \widehat{v} \in \mathcal{P}_{p-1}(\widehat{E}) \text{ for every edge } \widehat{E} \text{ of } \widehat{S}, \quad (20)$$

$$\int_{\widehat{S}} (\widehat{\Pi}_p \widehat{\phi} - \widehat{\phi}) \cdot \widehat{r} = 0, \quad \text{for all } \widehat{r} \in \mathcal{Q}_{p-1,p-2}(\widehat{S}) \times \mathcal{Q}_{p-2,p-1}(\widehat{S}). \quad (21)$$

The resulting discrete problem is given by (17), and its implementation will be discussed in the next subsection.

### 3.3. Implementation

We have implemented the method described by (17) and include here expanded forms for some of the deceptively simple expressions in (17) needed in the implementation. To solve (17), all of the functions

and integrals involved are restricted to a single element  $S_k$ , the resulting element matrix and load vector are constructed, and then assembled into a global system.

To facilitate the computation of the element matrix for element  $S_k$  from (17), we will begin by rewriting the bilinear form in (6) as

$$a(\vec{\phi}, \vec{\theta}) = 2 \int_{S_k} \left[ \frac{\partial \phi_1}{\partial x} \frac{\partial \theta_1}{\partial x} + \nu \left( \frac{\partial \phi_1}{\partial x} \frac{\partial \theta_2}{\partial y} + \frac{\partial \phi_2}{\partial y} \frac{\partial \theta_1}{\partial x} \right) + \frac{\partial \phi_2}{\partial y} \frac{\partial \theta_2}{\partial y} + \bar{\nu} \left( \frac{\partial \phi_1}{\partial y} + \frac{\partial \phi_2}{\partial x} \right) \left( \frac{\partial \theta_1}{\partial y} + \frac{\partial \theta_2}{\partial x} \right) \right] dx dy, \tag{22}$$

where  $\bar{\nu} = (1 - \nu)/2$ . Notice that this restatement leaves  $b$  unchanged

$$b(\vec{\phi}, w; \vec{\theta}, \zeta) = \int_{S_k} \left[ \left( \frac{\partial w}{\partial x} - \phi_1 \right) \left( \frac{\partial \zeta}{\partial x} - \theta_1 \right) + \left( \frac{\partial w}{\partial y} - \phi_2 \right) \left( \frac{\partial \zeta}{\partial y} - \theta_2 \right) \right] dx dy. \tag{23}$$

On each element, the solution is expanded as a linear combination of mapped basis functions  $\widehat{N}_i(\xi, \eta)$ , as follows:

$$\begin{aligned} \vec{\phi}(x, y) &= \vec{\phi}^0(x, y) + \vec{\phi}^e(x, y) \\ &= \sum_i J_k^{-T} \begin{pmatrix} \phi_1^i \\ \phi_2^i \end{pmatrix} \widehat{N}_i(\xi, \eta) + \sum_j \begin{pmatrix} \phi_1^j \\ \phi_2^j \end{pmatrix} \widehat{N}_j(\xi, \eta) \\ &= \sum_i \begin{pmatrix} \frac{\partial \xi}{\partial x} \phi_1^i + \frac{\partial \eta}{\partial x} \phi_2^i \\ \frac{\partial \xi}{\partial y} \phi_1^i + \frac{\partial \eta}{\partial y} \phi_2^i \end{pmatrix} \widehat{N}_i(\xi, \eta) + \sum_j \begin{pmatrix} \phi_1^j \\ \phi_2^j \end{pmatrix} \widehat{N}_j(\xi, \eta), \end{aligned}$$

where  $i$  indexes the internal, and  $j$  the external basis functions. Since we are interested in the  $p$  version, we utilize the hierarchical basis functions constructed from integrated Legendre polynomials (see Chapter 6 in [26] for details). In addition, this set of basis functions is naturally divided into external and internal functions, hence the non-traditional mapping of the internal basis functions does not further complicate the implementation of the method.

In order to plug the above expansion into (22) we will need expressions for the derivatives

$$\frac{\partial \phi_1}{\partial x} = \sum_j \phi_1^j \xi_{xx}^j + \phi_2^j \eta_{xx}^j, \quad \frac{\partial \phi_1}{\partial y} = \sum_j \phi_1^j \xi_{xy}^j + \phi_2^j \eta_{xy}^j, \tag{24}$$

$$\frac{\partial \phi_2}{\partial x} = \sum_j \phi_1^j \xi_{yx}^j + \phi_2^j \eta_{yx}^j, \quad \frac{\partial \phi_2}{\partial y} = \sum_j \phi_1^j \xi_{yy}^j + \phi_2^j \eta_{yy}^j, \tag{25}$$

where  $j$  now indexes all basis functions, and

$$\xi_{xx}^j = \begin{cases} \frac{\partial^2 \xi}{\partial x^2} \widehat{N}_j + \frac{\partial \xi}{\partial x} \frac{\partial \widehat{N}_j}{\partial x}, \\ \frac{\partial \widehat{N}_j}{\partial x}, \end{cases} \quad \eta_{xx}^j = \begin{cases} \frac{\partial^2 \eta}{\partial x^2} \widehat{N}_j + \frac{\partial \eta}{\partial x} \frac{\partial \widehat{N}_j}{\partial x}, \\ 0, \end{cases}$$

$$\xi_{xy}^j = \begin{cases} \frac{\partial^2 \xi}{\partial y \partial x} \widehat{N}_j + \frac{\partial \xi}{\partial x} \frac{\partial \widehat{N}_j}{\partial y}, \\ \frac{\partial \widehat{N}_j}{\partial y}, \end{cases} \quad \eta_{xy}^j = \begin{cases} \frac{\partial^2 \eta}{\partial y \partial x} \widehat{N}_j + \frac{\partial \eta}{\partial x} \frac{\partial \widehat{N}_j}{\partial y}, \\ 0, \end{cases}$$

$$\xi_{yx}^j = \begin{cases} \frac{\partial^2 \xi}{\partial x \partial y} \widehat{N}_j + \frac{\partial \xi}{\partial y} \frac{\partial \widehat{N}_j}{\partial x}, \\ 0, \end{cases} \quad \eta_{yx}^j = \begin{cases} \frac{\partial^2 \eta}{\partial x \partial y} \widehat{N}_j + \frac{\partial \eta}{\partial y} \frac{\partial \widehat{N}_j}{\partial x}, \\ \frac{\partial \widehat{N}_j}{\partial x}, \end{cases}$$

$$\xi_{yy}^j = \begin{cases} \frac{\partial^2 \xi}{\partial y^2} \widehat{N}_j + \frac{\partial \xi}{\partial y} \frac{\partial \widehat{N}_j}{\partial y}, \\ 0, \end{cases} \quad \eta_{yy}^j = \begin{cases} \frac{\partial^2 \eta}{\partial y^2} \widehat{N}_j + \frac{\partial \eta}{\partial y} \frac{\partial \widehat{N}_j}{\partial y}, \\ \frac{\partial \widehat{N}_j}{\partial y}, \end{cases}$$

(the top expressions are valid if  $j$  is the index of an internal basis function; the bottom expressions are valid otherwise). We will need to express these quantities as functions of the reference coordinates  $(\xi, \eta)$  in order to make a change of variables in integral (22). The first derivatives are obtained easily using the inverse function theorem

$$J_k^{-1}(x, y) = [J_k(\xi, \eta)]^{-1},$$

and explicitly inverting  $J_k$

$$\begin{bmatrix} \frac{\partial \xi}{\partial x} & \frac{\partial \xi}{\partial y} \\ \frac{\partial \eta}{\partial x} & \frac{\partial \eta}{\partial y} \end{bmatrix} = \begin{bmatrix} \frac{\partial x}{\partial \xi} & \frac{\partial x}{\partial \eta} \\ \frac{\partial y}{\partial \xi} & \frac{\partial y}{\partial \eta} \end{bmatrix}^{-1} = \frac{1}{|J_k|} \begin{bmatrix} \frac{\partial y}{\partial \eta} & -\frac{\partial x}{\partial \eta} \\ -\frac{\partial y}{\partial \xi} & \frac{\partial x}{\partial \xi} \end{bmatrix}.$$

Thus,

$$\frac{\partial \xi}{\partial x} = \frac{1}{|J_k|} \frac{\partial y}{\partial \eta}, \quad \frac{\partial \xi}{\partial y} = -\frac{1}{|J_k|} \frac{\partial x}{\partial \eta},$$

$$\frac{\partial \eta}{\partial x} = -\frac{1}{|J_k|} \frac{\partial y}{\partial \xi}, \quad \frac{\partial \eta}{\partial y} = \frac{1}{|J_k|} \frac{\partial x}{\partial \xi}.$$

From these expressions the second derivatives become

$$\frac{\partial^2 \xi}{\partial x^2} = +\frac{1}{|J_k|} \left[ \frac{\partial^2 y}{\partial \xi \partial \eta} \frac{\partial \xi}{\partial x} + \frac{\partial^2 y}{\partial \eta^2} \frac{\partial \eta}{\partial x} \right] - \frac{1}{|J_k|} \frac{\partial |J_k|}{\partial x} \frac{\partial \xi}{\partial x},$$

$$\frac{\partial^2 \xi}{\partial y \partial x} = +\frac{1}{|J_k|} \left[ \frac{\partial^2 y}{\partial \xi \partial \eta} \frac{\partial \xi}{\partial y} + \frac{\partial^2 y}{\partial \eta^2} \frac{\partial \eta}{\partial y} \right] - \frac{1}{|J_k|} \frac{\partial |J_k|}{\partial y} \frac{\partial \xi}{\partial x},$$

$$\frac{\partial^2 \xi}{\partial x \partial y} = -\frac{1}{|J_k|} \left[ \frac{\partial^2 x}{\partial \xi \partial \eta} \frac{\partial \xi}{\partial x} + \frac{\partial^2 x}{\partial \eta^2} \frac{\partial \eta}{\partial x} \right] - \frac{1}{|J_k|} \frac{\partial |J_k|}{\partial x} \frac{\partial \xi}{\partial y},$$

$$\frac{\partial^2 \xi}{\partial y^2} = -\frac{1}{|J_k|} \left[ \frac{\partial^2 x}{\partial \xi \partial \eta} \frac{\partial \xi}{\partial y} + \frac{\partial^2 x}{\partial \eta^2} \frac{\partial \eta}{\partial y} \right] - \frac{1}{|J_k|} \frac{\partial |J_k|}{\partial y} \frac{\partial \xi}{\partial y},$$

$$\frac{\partial^2 \eta}{\partial x^2} = -\frac{1}{|J_k|} \left[ \frac{\partial^2 y}{\partial \xi^2} \frac{\partial \xi}{\partial x} + \frac{\partial^2 y}{\partial \xi \partial \eta} \frac{\partial \eta}{\partial x} \right] - \frac{1}{|J_k|} \frac{\partial |J_k|}{\partial x} \frac{\partial \eta}{\partial x},$$

$$\frac{\partial^2 \eta}{\partial y \partial x} = -\frac{1}{|J_k|} \left[ \frac{\partial^2 y}{\partial \xi^2} \frac{\partial \xi}{\partial y} + \frac{\partial^2 y}{\partial \xi \partial \eta} \frac{\partial \eta}{\partial y} \right] - \frac{1}{|J_k|} \frac{\partial |J_k|}{\partial y} \frac{\partial \eta}{\partial x},$$

$$\frac{\partial^2 \eta}{\partial x \partial y} = +\frac{1}{|J_k|} \left[ \frac{\partial^2 x}{\partial \xi^2} \frac{\partial \xi}{\partial x} + \frac{\partial^2 x}{\partial \xi \partial \eta} \frac{\partial \eta}{\partial x} \right] - \frac{1}{|J_k|} \frac{\partial |J_k|}{\partial x} \frac{\partial \eta}{\partial y},$$

$$\frac{\partial^2 \eta}{\partial y^2} = +\frac{1}{|J_k|} \left[ \frac{\partial^2 x}{\partial \xi^2} \frac{\partial \xi}{\partial y} + \frac{\partial^2 x}{\partial \xi \partial \eta} \frac{\partial \eta}{\partial y} \right] - \frac{1}{|J_k|} \frac{\partial |J_k|}{\partial y} \frac{\partial \eta}{\partial y}.$$

Now, we separate the integrand from (22) into three parts

$$\int_{S_k} \left( \frac{\partial \phi_1}{\partial x} \frac{\partial \theta_1}{\partial x} + \frac{\partial \phi_2}{\partial y} \frac{\partial \theta_2}{\partial y} \right) dx dy = [\bar{\theta}_1 \ \bar{\theta}_2] \begin{bmatrix} G_{00} & G_{01} \\ G_{10} & G_{11} \end{bmatrix} \begin{bmatrix} \vec{\phi}_1 \\ \vec{\phi}_2 \end{bmatrix}, \tag{26}$$

$$\int_{S_k} \left( \frac{\partial \phi_1}{\partial x} \frac{\partial \theta_2}{\partial y} + \frac{\partial \phi_2}{\partial y} \frac{\partial \theta_1}{\partial x} \right) dx dy = [\bar{\theta}_1 \ \bar{\theta}_2] \begin{bmatrix} D_{00} & D_{01} \\ D_{10} & D_{11} \end{bmatrix} \begin{bmatrix} \vec{\phi}_1 \\ \vec{\phi}_2 \end{bmatrix}, \tag{27}$$

$$\int_{S_k} \left( \frac{\partial \phi_1}{\partial y} + \frac{\partial \phi_2}{\partial x} \right) \left( \frac{\partial \theta_1}{\partial y} + \frac{\partial \theta_2}{\partial x} \right) dx dy = [\bar{\theta}_1 \ \bar{\theta}_2] \begin{bmatrix} R_{00} & R_{01} \\ R_{10} & R_{11} \end{bmatrix} \begin{bmatrix} \vec{\phi}_1 \\ \vec{\phi}_2 \end{bmatrix}, \tag{28}$$

so that

$$a(\vec{\phi}, \vec{\theta}) = 2[\bar{\theta}_1 \ \bar{\theta}_2] \begin{bmatrix} G_{00} + \nu D_{00} + \bar{\nu} R_{00} & G_{01} + \nu D_{01} + \bar{\nu} R_{01} \\ G_{10} + \nu D_{10} + \bar{\nu} R_{10} & G_{11} + \nu D_{11} + \bar{\nu} R_{11} \end{bmatrix} \begin{bmatrix} \vec{\phi}_1 \\ \vec{\phi}_2 \end{bmatrix}.$$

Here,  $\vec{\phi}_1$  and  $\vec{\phi}_2$  are coefficient vectors for  $\phi_1$  and  $\phi_2$ . We will now show how to obtain expressions for the entries of the matrix  $G$  and state the analogous expressions for  $D$  and  $R$ . In the left-hand side of (26) we use the expansions in (24)–(25) for  $\vec{\phi}$  and analogous ones for  $\vec{\theta}$  to obtain

$$\begin{aligned} \frac{\partial \phi_1}{\partial x} \frac{\partial \theta_1}{\partial x} + \frac{\partial \phi_2}{\partial y} \frac{\partial \theta_2}{\partial y} &= \left( \sum_j \phi_1^j \xi_{xx}^j + \phi_2^j \eta_{xx}^j \right) \left( \sum_i \theta_1^i \xi_{xx}^i + \theta_2^i \eta_{xx}^i \right) \\ &\quad + \left( \sum_j \phi_1^j \xi_{yy}^j + \phi_2^j \eta_{yy}^j \right) \left( \sum_i \theta_1^i \xi_{yy}^i + \theta_2^i \eta_{yy}^i \right) \\ &= \sum_{i,j} \theta_1^i (\xi_{xx}^i \xi_{xx}^j + \xi_{yy}^i \xi_{yy}^j) \phi_1^j + \theta_1^i (\xi_{xx}^i \eta_{xx}^j + \xi_{yy}^i \eta_{yy}^j) \phi_2^j \\ &\quad + \theta_2^i (\eta_{xx}^i \xi_{xx}^j + \eta_{yy}^i \xi_{yy}^j) \phi_1^j + \theta_2^i (\eta_{xx}^i \eta_{xx}^j + \eta_{yy}^i \eta_{yy}^j) \phi_2^j. \end{aligned}$$

Similarly, the right-hand side of (26) can be expanded as

$$\begin{aligned} & \bar{\theta}_1 G_{00} \bar{\phi}_1 + \bar{\theta}_1 G_{01} \bar{\phi}_2 + \bar{\theta}_2 G_{10} \bar{\phi}_1 + \bar{\theta}_2 G_{11} \bar{\phi}_2 \\ &= \sum_{i,j} \theta_1^i [G_{00}]_{ij} \phi_1^j + \theta_1^i [G_{01}]_{ij} \phi_2^j + \theta_2^i [G_{10}]_{ij} \phi_1^j + \theta_2^i [G_{11}]_{ij} \phi_2^j. \end{aligned}$$

By matching terms in the previous two sums and changing variables in the integrals in (26) we obtain

$$[G_{00}]_{ij} = \int_{\hat{S}} (\xi_{xx}^i \xi_{xx}^j + \xi_{yy}^i \xi_{yy}^j) |J_k| d\xi d\eta,$$

$$[G_{01}]_{ij} = \int_{\hat{S}} (\xi_{xx}^i \eta_{xx}^j + \xi_{yy}^i \eta_{yy}^j) |J_k| d\xi d\eta,$$

$$[G_{10}]_{ij} = \int_{\hat{S}} (\eta_{xx}^i \xi_{xx}^j + \eta_{yy}^i \xi_{yy}^j) |J_k| d\xi d\eta,$$

$$[G_{11}]_{ij} = \int_{\hat{S}} (\eta_{xx}^i \eta_{xx}^j + \eta_{yy}^i \eta_{yy}^j) |J_k| d\xi d\eta.$$

By similar means

$$[D_{00}]_{ij} = \int_{\hat{S}} (\xi_{yy}^i \xi_{xx}^j + \xi_{xx}^i \xi_{yy}^j) |J_k| d\xi d\eta,$$

$$[D_{01}]_{ij} = \int_{\hat{S}} (\xi_{yy}^i \eta_{xx}^j + \xi_{xx}^i \eta_{yy}^j) |J_k| d\xi d\eta,$$

$$[D_{10}]_{ij} = \int_{\hat{S}} (\eta_{yy}^i \xi_{xx}^j + \eta_{xx}^i \xi_{yy}^j) |J_k| d\xi d\eta,$$

$$[D_{11}]_{ij} = \int_{\hat{S}} (\eta_{yy}^i \eta_{xx}^j + \eta_{xx}^i \eta_{yy}^j) |J_k| d\xi d\eta,$$

$$[R_{00}]_{ij} = \int_{\hat{S}} (\xi_{yx}^i + \xi_{xy}^i) (\xi_{yx}^j + \xi_{xy}^j) |J_k| d\xi d\eta,$$

$$[R_{01}]_{ij} = \int_{\hat{S}} (\xi_{yx}^i + \xi_{xy}^i) (\eta_{yx}^j + \eta_{xy}^j) |J_k| d\xi d\eta,$$

$$[R_{10}]_{ij} = \int_{\hat{S}} (\eta_{yx}^i + \eta_{xy}^i) (\xi_{yx}^j + \xi_{xy}^j) |J_k| d\xi d\eta,$$

$$[R_{11}]_{ij} = \int_{\hat{S}} (\eta_{yx}^i + \eta_{xy}^i) (\eta_{yx}^j + \eta_{xy}^j) |J_k| d\xi d\eta.$$

The global linear system is constructed from the above elemental expressions in the usual manner (including possibly static condensation [26]). For additional implementational details see [15].

#### 4. Numerical experiments

In this section we present the results of numerical computations for two model problems with known exact solutions [5], in order to accurately assess the performance of the method. The results presented here are for a unit circular plate with Young’s modulus  $E = 1$ , Poisson ratio  $\nu = 0.3$ , shear correction factor  $\kappa = 1$ , and transverse load density given in polar coordinates by

$$g(r, \theta) = \cos(\theta).$$

The mesh (shown in Fig. 1) was designed according to the recommendations of [20] and it includes thin elements of width  $pt$  along the boundary of the domain in order for the boundary layer to be uniformly approximated.<sup>1</sup> Here  $p$  is the degree of the approximating polynomial, which is increased from  $p = 1$  to 8 for our computations, and  $t$  is the plate thickness which was chosen as  $t = 10^{-j}$ ,  $j = 2, 3, 4$ . We note that no approximation to the boundary of the plate is made, but rather the curved elements are mapped exactly, using the blending map technique (cf. [26, pp. 107–108]) to construct the element mappings  $F_k$ . For simplicity, we have only implemented the method for quadrilateral elements, even though the implementation can be modified for triangular elements in a straight-forward manner.

We will be plotting the error measured in the energy norm

$$\|(\vec{\phi}, w)\|_E^2 = \frac{D}{2} a(\vec{\phi}, \vec{\phi}) + G\kappa t^{-2} b(\vec{\phi}, w; \vec{\phi}, w) \tag{29}$$

versus the number of degrees of freedom  $N$ , in a semi-log scale, as calculated using the  $p$ -MITC and the standard finite element method. In addition to (29), we are also interested in the pointwise error in the stress and moment resultants, and for concreteness we will concentrate on the approximation of the shear force, given by (4). For the MITC formulation the shear force will be computed using

$$\vec{Q}_N = -G\kappa t^{-2} (\vec{\nabla} w_N - \mathbf{\Pi}_N \vec{\phi}_N), \tag{30}$$

while for the standard formulation the shear force will be computed using the constitutive relation (4), as well as the equilibrium equation, which basically amounts to a post-processing scheme—the computations for this last case will be performed using the commercial finite element code StressCheck (E.S.R.D., St. Louis, MO). We should point out that  $\vec{Q}_N$  given by (30) is often referred to as *projected shear* (cf. [2]), and it gives a better approximation than the one obtained by Eq. (4) (with  $w, \vec{\phi}$  replaced by  $w_N, \vec{\phi}_N$ ); see [22] for details. The fact that the projection operator  $\mathbf{\Pi}_N$  is an integral part of the MITC formulation is the reason we do not refer to this as “post-processing”.

Since  $\vec{Q} \notin L^2(\Omega)$  as  $t \rightarrow 0$ , one cannot expect pointwise approximations to have any accuracy uniformly in  $t$ , especially near the boundary. For this reason we will compute  $\vec{Q}$  sufficiently away from the boundary; in particular we will be measuring the first component of the shear force  $Q_x(x, 0)$ , for  $0 \leq x \leq 1 - pt$ , with  $p = 8$  (the highest approximating polynomial degree).

---

<sup>1</sup> If the boundary layer is not well approximated then any computed results will not be accurate uniformly in  $t$ ; this occurs when, e.g., a uniform mesh is used (cf. [20,27]).

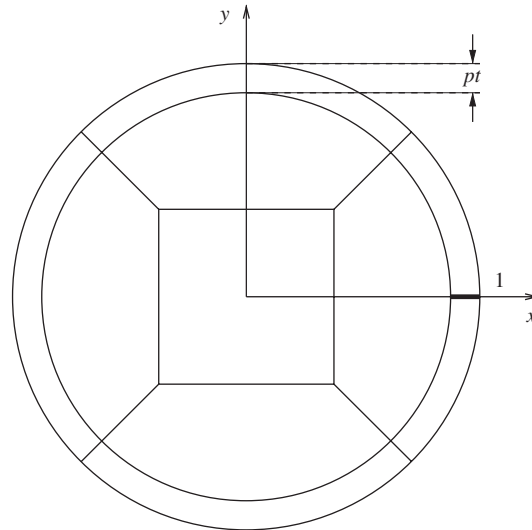


Fig. 1. 9-element unit-circular mesh with boundary refinement.

#### 4.1. Clamped plate

First we consider a clamped plate, for which the boundary layer is weak [6]. Figs. 2–4 show the error measured in the energy norm, as computed by both the standard and MITC formulations. As these figures indicate, both methods perform well, independently of the thickness  $t$ , and near exponential convergence rates are observed, with the relative error being reduced down to 1%. (These rates can also be interpreted as arbitrarily high algebraic convergence.)

Figs. 5–7 show the shear force distribution, as well as the error in the shear force, for the standard formulation (with and without post-processing) and for the MITC formulation. First, we note that for  $t = 0.01$  (see Fig. 5) most of the error comes from the center of the plate, while as  $t$  gets smaller (see Figs. 6 and 7) the error closer to the boundary dominates—this is more so for the standard formulation(s) than for the MITC method. This is due to the fact that the mesh (see Fig. 1) is coarse and only one element is used in the middle of the plate. Even though adding more elements in the interior would improve the situation for all methods, we see that the MITC formulation performs quite well without additional refinement.

These figures also confirm that post-processing the FEM solution is *necessary* if one uses the standard formulation (especially as  $t \rightarrow 0$ ). But most importantly, they show that the MITC formulation performs at least as well as the standard formulation with post-processing, and visibly better as  $t \rightarrow 0$ , without the need for additional post-processing (beyond the fact that (30) is used).

Finally, Fig. 8 shows the convergence of the computed shear at the center of the plate, for both the standard formulation with post-processing and the  $p$ -MITC formulation. In particular, we plot the percentage relative error in  $Q_x(0, 0)$ , versus the polynomial degree  $p$  in a semilog scale, for  $t = 0.01$  (for different thickness, the plots are similar to the one shown here). We see that both methods converge at an observed near exponential rate, with the  $p$ -MITC method having a slight advantage. (See also [22,2] for  $L^2$  error

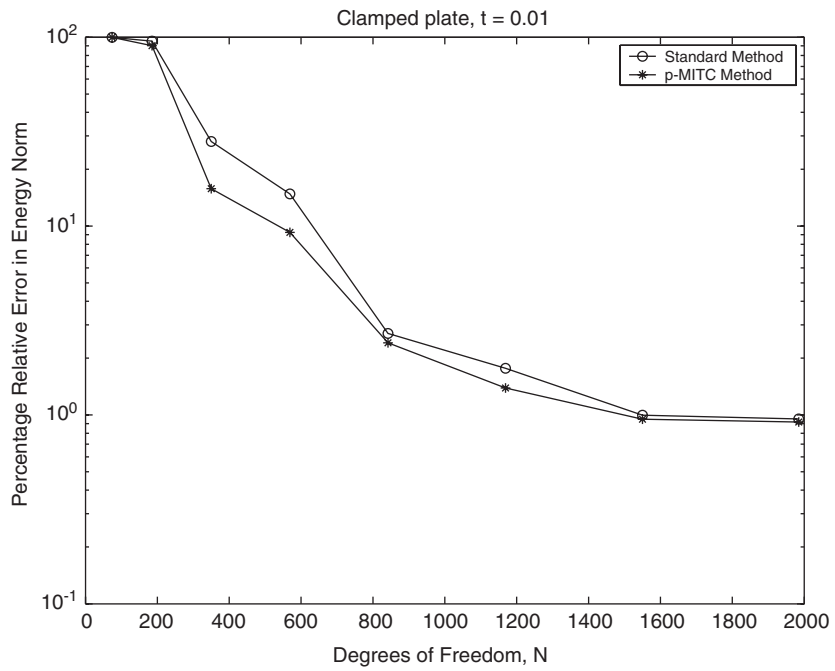


Fig. 2. Energy norm convergence for the clamped plate,  $t = 0.01$ .

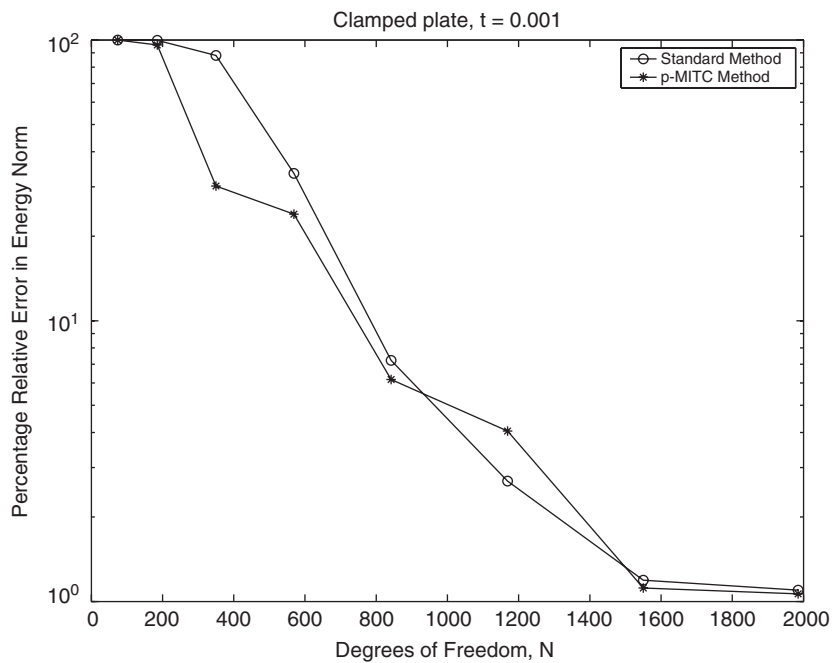


Fig. 3. Energy norm convergence for the clamped plate,  $t = 0.001$ .

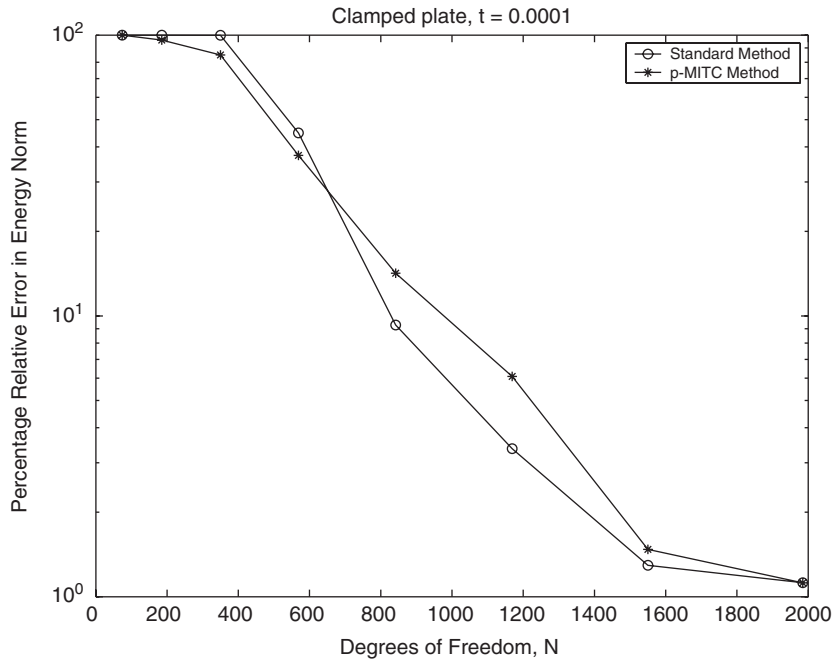


Fig. 4. Energy norm convergence for the clamped plate,  $t = 0.0001$ .

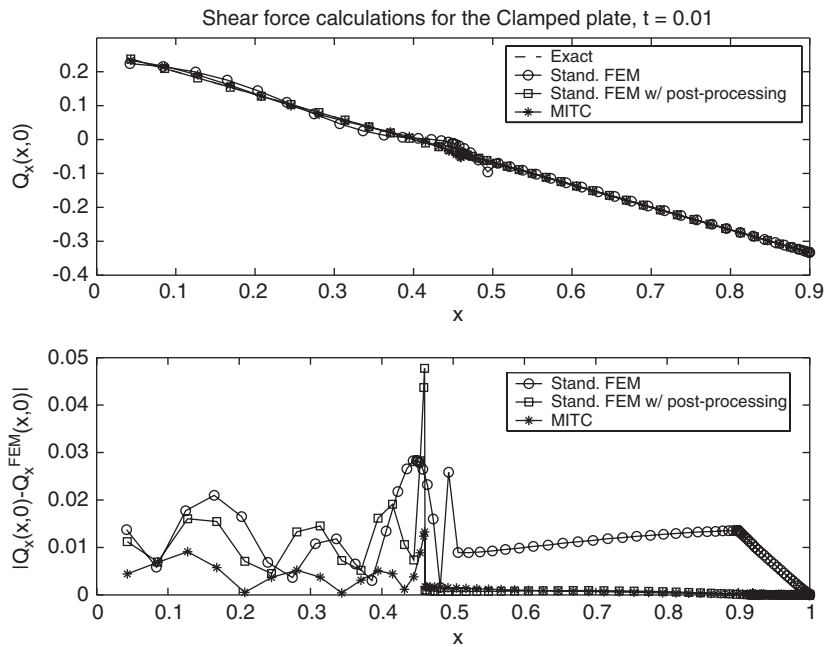


Fig. 5. Shear force computations for the clamped plate,  $t = 0.01$ .

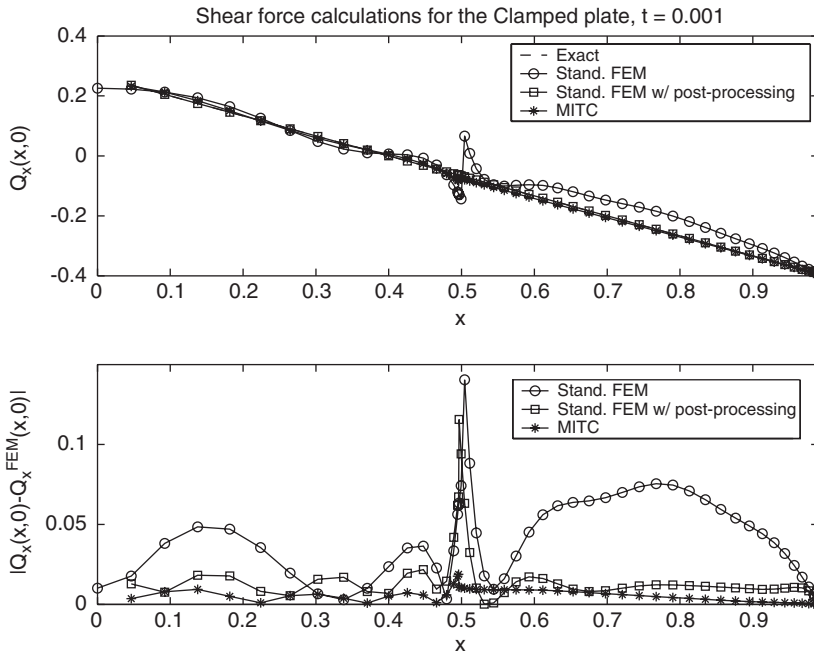


Fig. 6. Shear force computations for the clamped plate,  $t = 0.001$ .

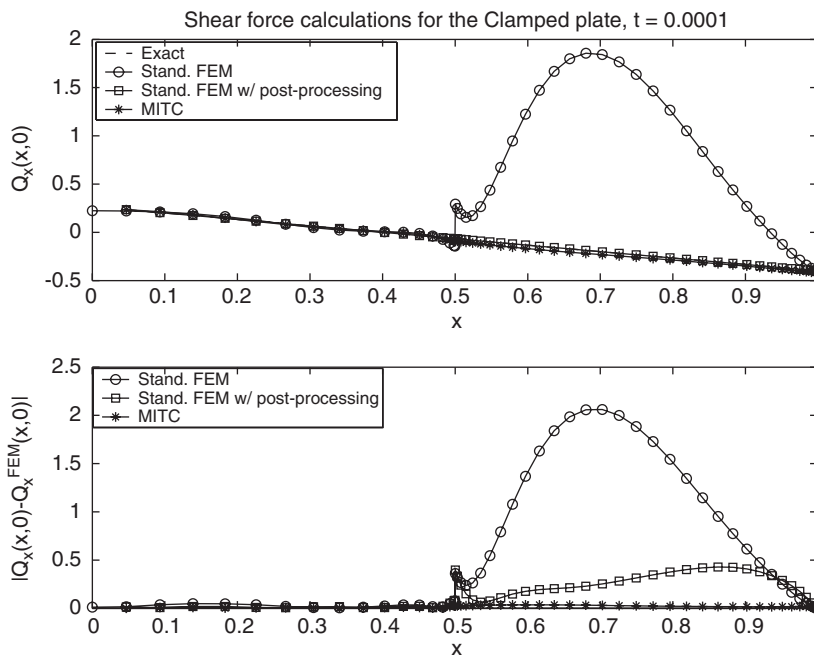


Fig. 7. Shear force computations for the clamped plate,  $t = 0.0001$ .

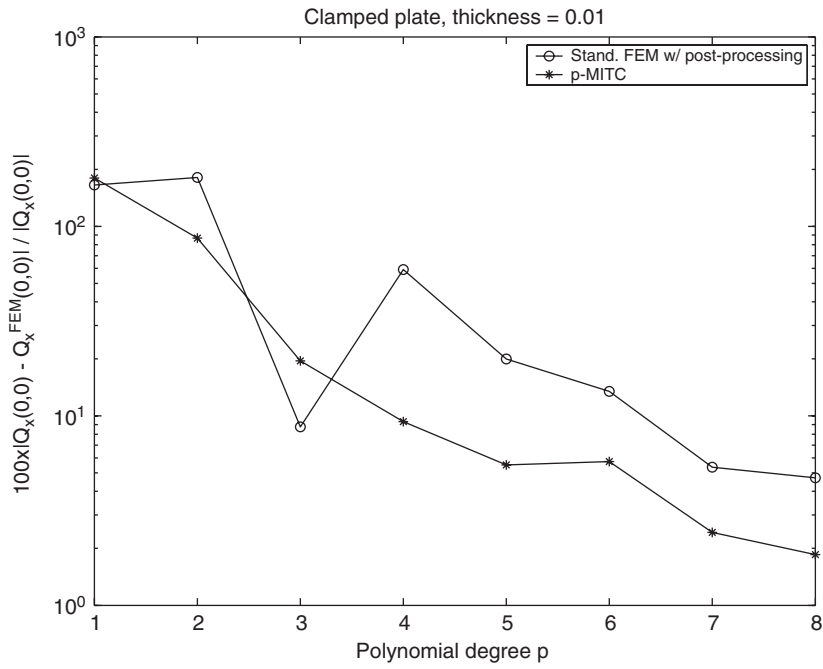


Fig. 8. Convergence of the shear force at (0,0) for the clamped plate,  $t = 0.01$ .

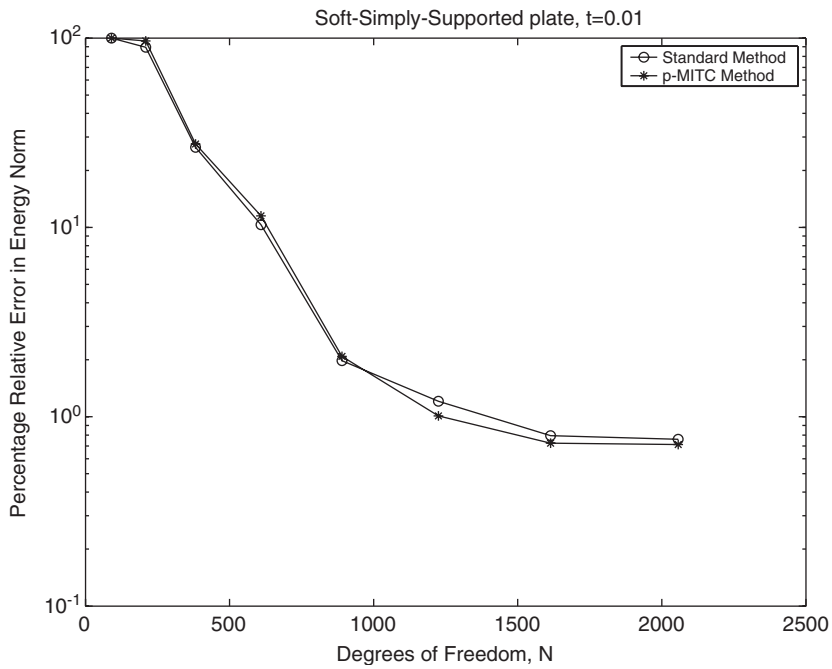


Fig. 9. Energy norm convergence for the S–S–S plate,  $t = 0.01$ .

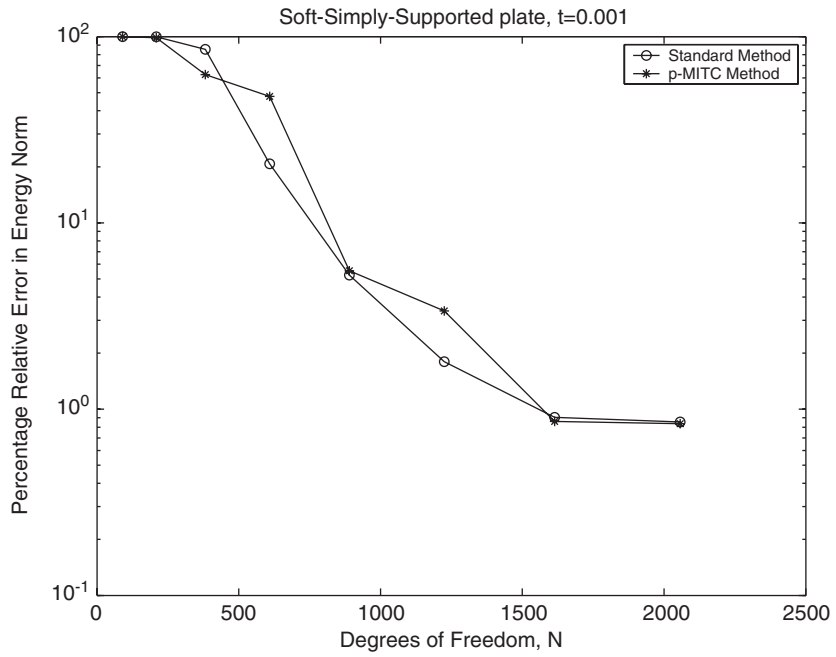


Fig. 10. Energy norm convergence for the S–S–S plate,  $t = 0.001$ .

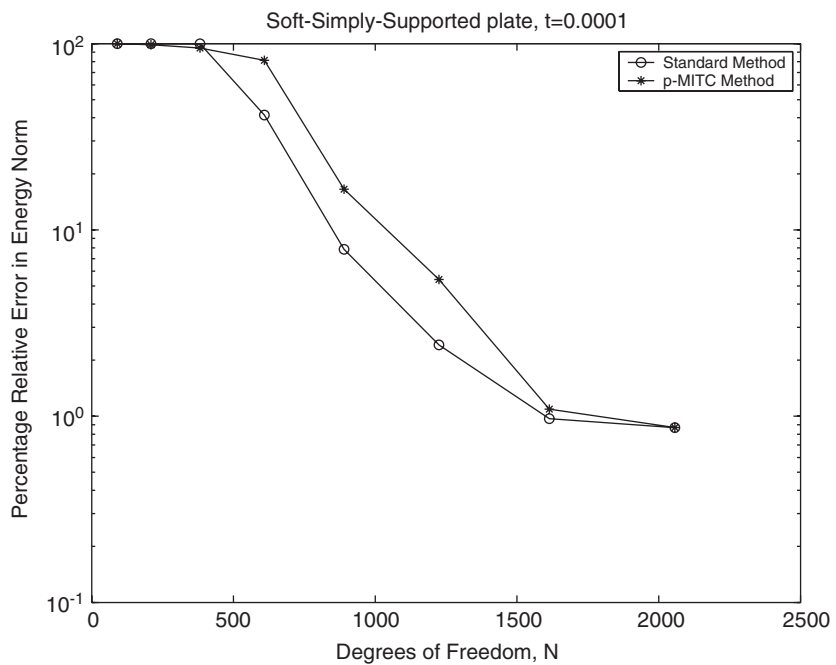


Fig. 11. Energy norm convergence for the S–S–S plate,  $t = 0.0001$ .

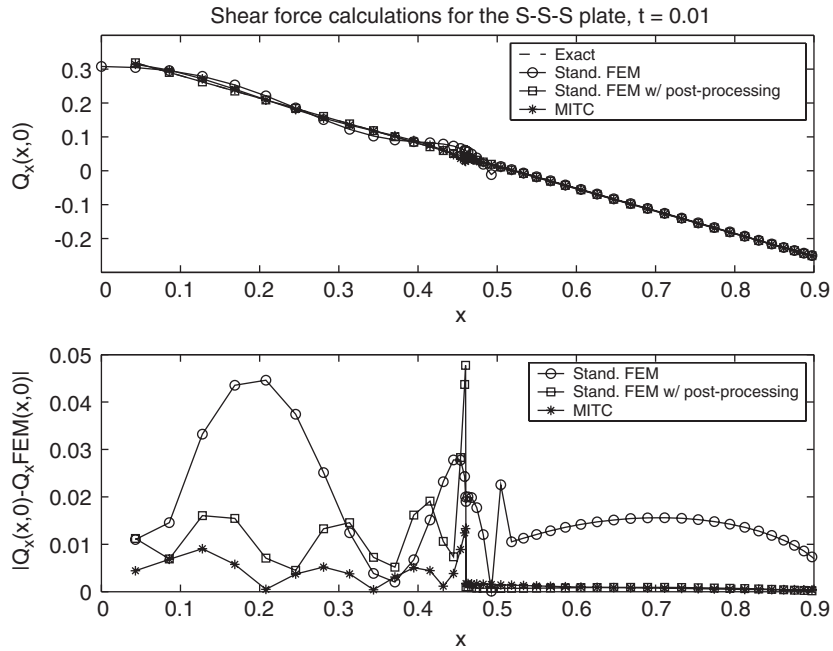


Fig. 12. Shear force computations for the S-S-S plate,  $t = 0.01$ .

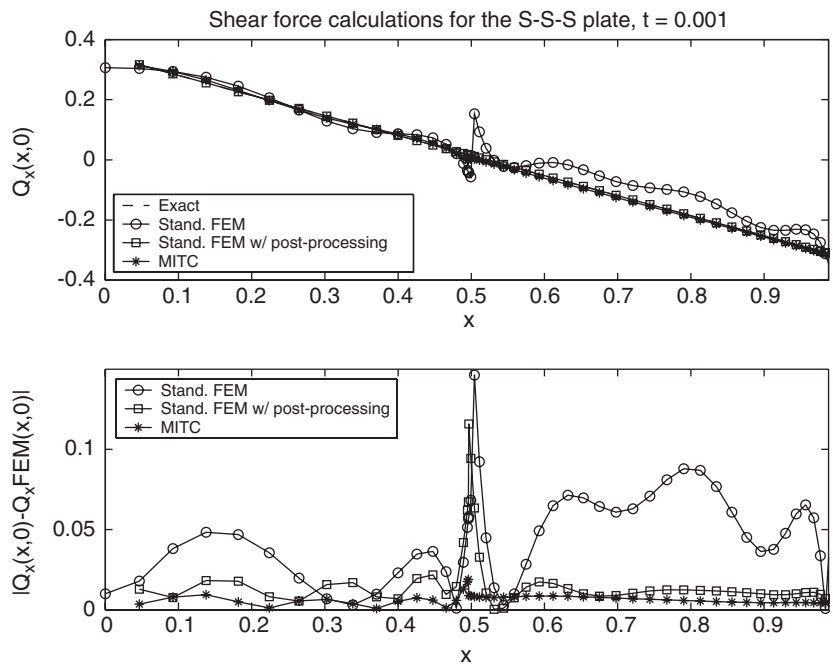


Fig. 13. Shear force computations for the S-S-S plate,  $t = 0.001$ .

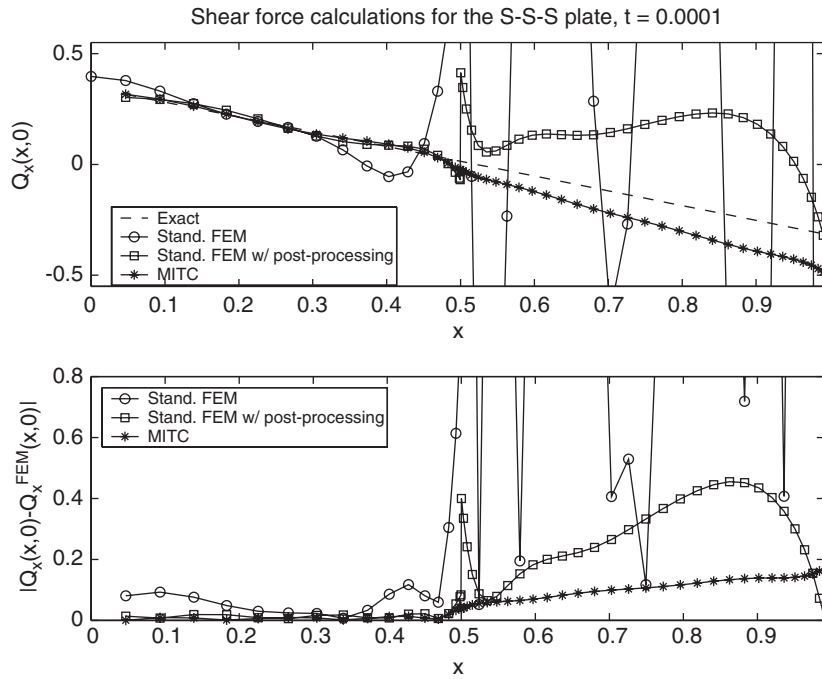


Fig. 14. Shear force computations for the S–S–S plate,  $t = 0.0001$ .

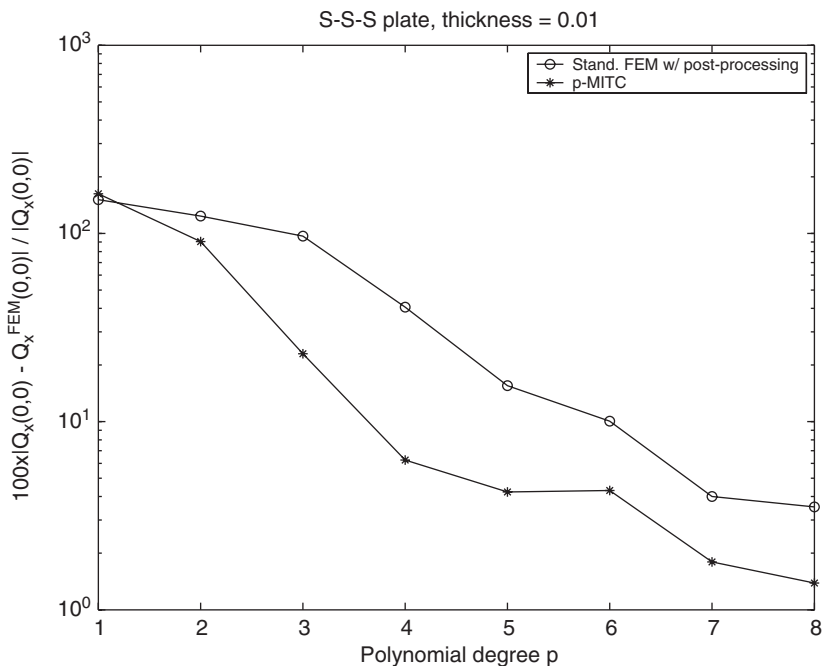


Fig. 15. Convergence of the shear force at  $(0,0)$  for the S–S–S plate,  $t = 0.01$ .

estimates for the shear in the case of quasiuniform, and locally quasiuniform meshes with straight sided elements.)

#### 4.2. Soft-simply-supported plate

We now repeat the previous experiments for the case of a soft-simply-supported plate, keeping all material constants and loads the same as before. In this case the boundary layer is stronger [4], hence the proper mesh design is of utmost importance (cf. [20]). Figs. 9–11 show the energy norm convergence for both methods and, as before, we observe that their performance is not affected by  $t \rightarrow 0$  and all three seem to be converging near exponentially, with the error reduced down to 1%.

The shear force (and the associated errors) are shown in Figs. 12–14. With the exception of  $t = 0.0001$ , the results are almost identical to the previous example, and once again confirm that MITC methods are excellent for the approximation of plate problems, even in the presence of curved elements. For  $t = 0.0001$  (see Fig. 14) we see that the standard formulation without post-processing yields extremely high errors, while the performance of the other two methods begins to deteriorate as we get closer to the boundary, due to the lack of smoothness of  $Q_x$ .

Finally, Fig. 15 shows the convergence for the standard and MITC formulations, as was done in the previous example, with identical conclusions.

### 5. Conclusions

We have studied the approximation of the Reissner–Mindlin plates with curved boundaries by a  $p$  version MITC finite element method. By combining the ideas of [22] on  $hp$  MITC methods and of [13] on curved elements, we were able to successfully formulate and implement the method. Our numerical computations confirmed that  $p$ -MITC elements are extremely effective for plate problems, even when curved elements are used, provided that certain care is taken in constructing the element mappings. This information should prove to be quite useful if one is interested in the more difficult *shell* problem, for which the use of curved elements (and MITC formulations) is pivotal [7].

### References

- [1] M. Ainsworth, P. Coggins, The stability of mixed  $hp$  finite element methods for Stokes flow on high aspect ratio elements, *SIAM J. Numer. Anal.* 38 (2000) 1721–1761.
- [2] M. Ainsworth, K. Pichedez,  $hp$ -MITC finite element method for the Reissner–Mindlin plate problem, *J. Comput. Appl. Math.* 148 (2002) 429–462.
- [3] M. Ainsworth, K. Pichedez,  $hp$ -Approximation theory for BDFM/RT finite elements and applications, *SIAM J. Numer. Anal.* 40 (2002) 2047–2068.
- [4] D. Arnold, R. Falk, A uniformly accurate finite element method for the Reissner–Mindlin plate, *SIAM J. Numer. Anal.* 26 (1989) 1276–1290.
- [5] D. Arnold, R. Falk, Edge effects in the Reissner–Mindlin plate theory, in: A.K. Noor, T. Belytschko, J.C. Simo (Eds.), *Analytic and Computational Models of Shells*, A.S.M.E., New York, 1989, pp. 71–90.
- [6] D. Arnold, R. Falk, Asymptotic analysis of the boundary layer for the Reissner–Mindlin plate model, *SIAM J. Numer. Anal.* 34 (1996) 544–568.
- [7] K.J. Bathe, A. Iosilevich, D. Chapelle, An evaluation of the MITC shell elements, *Comput. Struct.* 75 (2000) 1–30.

- [8] F. Brezzi, K.J. Bathe, M. Fortin, Mixed-interpolated elements for Reissner–Mindlin plates, *Int. J. Numer. Meth. Eng.* 28 (1989) 1787–1801.
- [9] F. Brezzi, J. Douglas Jr., M. Fortin, D. Marini, Efficient rectangular mixed finite elements in two and three space variables, *RAIRO  $M^2AN$*  21 (1987) 237–250.
- [10] F. Brezzi, M. Fortin, Numerical approximation of Mindlin–Reissner plates, *Math. Comp.* 47 (1986) 151–158.
- [11] F. Brezzi, M. Fortin, *Mixed and Hybrid Finite Element Methods*, Springer, Berlin, 1991.
- [12] L.K. Chilton, Locking free mixed  $hp$  finite element methods for linear and geometrically nonlinear elasticity, Ph.D. Dissertation, University of Maryland, Baltimore County, 1997.
- [13] L. Chilton, M. Suri, On the construction of stable curvilinear  $p$  version elements for mixed formulations of elasticity and Stokes flow, *Numer. Math.* 86 (2000) 29–48.
- [14] S. Fulton, J. Kurtz, C. Xenophontos, On the uniform approximation of the Reissner–Mindlin plate model by  $p/hp$  finite element methods, in: H.A. Mang, F.G. Rammerstorfer, J. Eberhardsteiner (Eds.), *Proceedings of the Fifth World Congress on Computational Mechanics (WCCM V)*, July 7–12, 2002, Vienna, Austria, ISBN: 3-9501554-0-6.
- [15] J. Kurtz, A  $p$  Version Finite Element Method for Shear Force Computation in Reissner–Mindlin Plates with Curved Boundary, M.Sc. Thesis, Department of Mathematics and Computer Science, Clarkson University, Potsdam NY, May 2002.
- [16] J. Kurtz, C. Xenophontos, On the effects of using curved elements in the approximation of the Reissner–Mindlin plate by the  $p$  version of the finite element method, *Appl. Numerical Math.* 46 (2003) 231–246.
- [17] E. Rank, R. Krausse, K. Preusch, On the accuracy of  $p$ -version elements for the Reissner–Mindlin plate model, *Int. J. Numer. Meth. Eng.* 43 (1998) 51–67.
- [18] P.A. Raviart, J.M. Thomas, A mixed finite element method for second order elliptic problems, *Mathematical Aspects of the Finite Element Method*, Lecture Notes in Mathematics, vol. 606, Springer, NY, 1977, pp. 292–315.
- [19] D. Schötzau, C. Schwab, Mixed  $hp$ -finite element methods on anisotropic meshes, *Math. Meth. Appl. Sci.* 8 (1998) 787–820.
- [20] Ch. Schwab, M. Suri, C. Xenophontos, The  $hp$  finite element method for problems in mechanics with boundary layers, *Comput. Methods Appl. Mech. Eng.* 157 (1998) 311–333.
- [21] R. Stenberg, M. Suri, Mixed  $hp$  finite elements for elasticity and Stokes flow, *Numer. Math.* 72 (1996) 367–389.
- [22] R. Stenberg, M. Suri, An  $hp$  error analysis of MITC plate elements, *SIAM J. Numer. Anal.* 34 (1997) 544–568.
- [23] M. Suri, Analytic and computational assessment of locking in the  $hp$  finite element method, *Comput. Meth. Appl. Mech. Eng.* 133 (1996) 347–371.
- [24] M. Suri, I. Babuška, Ch. Schwab, Locking effects in the finite element approximation of plate models, *Math. Comp.* 64 (1995) 461–482.
- [25] M. Suri, Ch. Schwab, Locking and boundary layer effects in the finite element approximation of the Reissner–Mindlin plate model, *Proc. Symp. Appl. Math.* 48 (1994) 367–371.
- [26] B. Szabó, I. Babuška, *Finite Element Analysis*, Wiley, NY, 1991.
- [27] C. Xenophontos, Finite element computations for the Reissner–Mindlin plate model, *Comm. Numer. Meth. Eng.* 14 (1998) 1119–1131.